

# The Presence of Sterols Favors Sticholysin I-Membrane Association and Pore Formation Regardless of Their Ability to Form Laterally Segregated Domains

Lohans Pedrera,<sup>†</sup> Andreza B. Gomide,<sup>‡,§</sup> Rafael E. Sánchez,<sup>†</sup> Uris Ros,<sup>†</sup> Natalia Wilke,<sup>||</sup> Fabiola Pazos,<sup>†</sup> María E. Lanio,<sup>†</sup> Rosangela Itri,<sup>‡</sup> María Laura Fanani,<sup>||</sup> and Carlos Alvarez<sup>\*,†</sup>

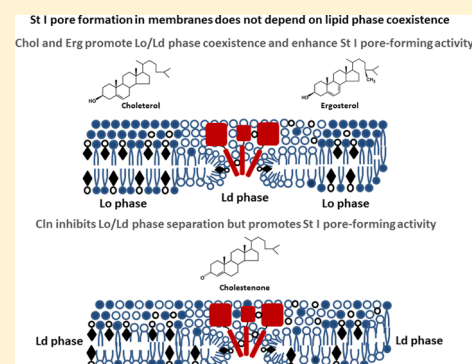
<sup>†</sup>Centro de Estudio de Proteínas (CEP), Facultad de Biología, Universidad de la Habana, CP 10400, La Habana, Cuba

<sup>‡</sup>Departamento de Física Aplicada, Instituto de Física, Universidade de São Paulo, 05508090, São Paulo, Brasil

<sup>§</sup>Centro Universitário Padre Anchieta, Jundiaí, 13207270, São Paulo, Brasil

<sup>||</sup>Departamento de Química Biológica, Centro de Investigaciones en Química Biológica de Córdoba (CIQUIBIC), Facultad de Ciencias Químicas-CONICET, Universidad Nacional de Córdoba, X5000HUA Córdoba, Argentina

**ABSTRACT:** Sticholysin I (St I) is a pore-forming toxin (PFT) produced by the Caribbean Sea anemone *Stichodactyla helianthus* belonging to the actinoporin protein family, a unique class of eukaryotic PFT. As for actinoporins, it has been proposed that the presence of cholesterol (Chol) and the coexistence of lipid phases increase binding to the target membrane and pore-forming ability. However, little is known about the role of membrane structure and dynamics (phase state, fluidity, and the presence of lipid domains) on the activity of actinoporins or which regions of the membrane are the most favorable for protein insertion, oligomerization, and eventually pore formation. To gain insight into the role of membrane properties on the functional activity of St I, we studied its binding to monolayers and vesicles of phosphatidylcholine (PC), sphingomyelin (SM), and sterols inducing (ergosterol -Erg and cholesterol -Chol) or not (cholestenone -Cln) membrane phase segregation in liquid ordered (Lo) and liquid disordered (Ld) domains. This study revealed that St I binds and permeabilizes with higher efficiency sterol-containing membranes independently of their ability to form domains. We discuss the results in terms of the relevance of different membrane properties for the actinoporins mechanism of action, namely, molecular heterogeneity, specially potentiated in membranes with sterols inducers of phase separation (Chol or Erg) or Cln, a sterol noninducer of phase separation but with a high propensity to induce nonlamellar phase. The role of the Ld phase is pointed out as the most suitable platform for pore formation. In this regard, such regions in Chol-containing membranes seem to be the most favored due to its increased fluidity; this property promotes toxin insertion, diffusion, and oligomerization leading to pore formation.



## 1. INTRODUCTION

Sea anemones produce a wide variety of toxins that act together as essential tools to capture prey or defend from predators. Their toxin arsenal includes neurotoxins,<sup>1,2</sup> phospholipases,<sup>3,4</sup> protease inhibitors,<sup>5</sup> and pore-forming toxins (PFTs).<sup>6–8</sup> The formation of pores by PFTs can be achieved by inserting either  $\alpha$ -helices or  $\beta$ -hairpins within the target membrane, property that has been employed to classify them into two well-defined groups:  $\alpha$ -PFTs and  $\beta$ -PFTs, respectively.<sup>9,10</sup> Actinoporins are  $\alpha$ -PFTs exclusively found in sea anemones made of a single polypeptide chain, with molecular weight around 20 kDa and whose lipidic receptor in the membrane is SM.<sup>8</sup> To date, the most studied actinoporins are equitoxin II (Eqt II) from *Actinia equina*,<sup>11,12</sup> St I and sticholysin II (St II), two isoforms produced by *Stichodactyla helianthus*,<sup>13</sup> and fragaceatoxin C (FraC) synthesized by *Actinia fragacea*.<sup>14</sup> The mechanism of pore formation proposed for actinoporins is based on an initial binding step followed by oligomerization and membrane insertion leading to pore formation.<sup>15–17</sup>

Over recent years it has been postulated that the affinity of actinoporins for membranes is greatly enhanced by the coexistence of lipid phases.<sup>18–23</sup> In model lipid systems, Lo domains are usually formed when Chol associates with saturated glycerol- or sphingo-phospholipids rendering phospholipid–Chol complexes.<sup>24</sup> In particular, SM has emerged as an important partner of Chol for Lo phase formation, and ternary mixtures of dioleoylphosphatidylcholine (DOPC), SM, and Chol have become one of the most studied model membrane systems exhibiting Lo/Ld phase coexistence.<sup>24</sup> In this regard, Lo and Ld phases in bilayers or their equivalent Lo and liquid expanded (Le) phases in monolayers, have been the most studied systems in the actinoporin family.<sup>18–20,22,23</sup> In fact, packing defects related to the occurrence of lipid microdomains have been claimed as a preferential binding

Received: May 7, 2015

Revised: August 10, 2015

site for Eqt II.<sup>18,20</sup> More recently, for Eqt II it was proposed that domain boundaries between Lo and Ld phases act as preferential binding sites before the toxin accumulates in the Ld phase, where the pore-formation takes place predominantly.<sup>22</sup> These new observations are in conflict with previous ones that suggested the preference of Eqt II for Lo phase.<sup>20</sup> In line with this evidence, we demonstrated that St I binds and penetrates with faster kinetic lipid monolayers with high lateral mobility regardless of the presence of isolated condensed domains or high proportion of SM.<sup>25</sup> Hence, the interplay between actinoporins and membrane is a complex process and still far from being completely understood. In a general sense, there is a lack of data allowing one to generalize that more fluid lipidic platforms are the most suitable regions of membrane for pore-formation by actinoporins or whether such observations depend on the model system and lipid composition employed, a common problem in membrane biophysics.

Since the effect of Lo/Ld phase coexistence on St I functional activity has been barely explored, here we investigate how the presence of three different sterols—Chol, Erg, and Cln—impact on St I membrane binding and pore-forming activity by modulating the phase state of the membrane. Chol is one of the major lipids of mammalian membranes, whereas Erg is characteristically found in yeast and fungi membrane.<sup>26</sup> Both Chol and Erg are promoters of liquid phase coexistence in phospholipid membranes whereas Cln, the main catabolic product of Chol oxidase (EC 1.1.3.6) in the bile acid biosynthesis pathway,<sup>27</sup> is an inhibitor.<sup>26,28</sup> To this end, we have compared St I behavior on lipid monolayers and vesicles composed of ternary mixtures of DOPC:SM:sterol (1:1:1). We demonstrated that sterols increase the binding and pore-forming activity of St I independently of the sterol ability to generate Lo domains.

## 2. MATERIALS AND METHODS

**2.1. Chemicals and Reagents.** St I was purified from the sea anemone *S. helianthus* by combining gel filtration chromatography on Sephadex G-50 medium (Pharmacia-LKB, Sweden) and cationic exchange chromatography on CM-cellulose S2 (Whatman, Maidstone, UK) as described.<sup>13</sup> The lipids DOPC, egg SM, and Chol were purchased from Avanti Polar Lipids (Alabaster, AL, USA) while Erg and Cln were from Sigma-Aldrich (USA). The lipophilic fluorescent probe  $\alpha$ -phosphatidylethanolamine-*N*-lissamine rhodamine B sulfonyl-ammonium salt, chicken egg-transphosphatidylated (Rho-PE), the amine-reactive probe Alexa Fluor 488 carboxylic acid succinimidyl ester, and carboxyfluorescein (CF) were obtained from Invitrogen (Eugene, OR, USA). Solvents and chemicals were of the highest commercial purity available. Water was purified by a Milli-Q system (Millipore, Billerica, MA, USA), to yield a product with a resistivity of  $\sim 18.5 \text{ M}\Omega\cdot\text{cm}^{-1}$ . For monolayer assays, the absence of surface active impurities was routinely checked as described elsewhere.<sup>29</sup>

**2.2. Binding of St I to Lipid Monolayers.** Surface pressure measurements were carried out with a  $\mu$ Trough-S system (Kibron, Helsinki, Finland) at room temperature ( $23 \pm 2^\circ\text{C}$ ) under constant stirring. The subphase consisted of 300  $\mu\text{L}$  of Tris-buffered saline solution (TBS: 145 mM NaCl, 10 mM Tris-HCl, pH 7.4). The lipid mixture dissolved in chloroform:methanol (2:1, v:v) was gently spread over the surface, and the desired initial surface pressure ( $\pi_0$ ) was attained by changing the amount of lipid applied to the air–water interface. After 5 min for allowing solvent evaporation, St I was injected into the subphase to achieve 0.8  $\mu\text{M}$  protein final concentration. At this subphase concentration, St I has no effect on surface tension of the air–buffer interface. The increment in surface pressure ( $\Delta\pi$ ) was recorded as a function of the elapsed time until a stable signal was obtained.

**2.3. Monolayer Compression Isotherms.** Compression–expansion isotherms were obtained by spreading 25  $\mu\text{L}$  of chloroform:methanol (2:1, v:v) lipid solution onto a Teflon trough filled with TBS. The film was relaxed for 5 min at  $0 \text{ mN}\cdot\text{m}^{-1}$  and subsequently compressed at a rate of  $1 \text{ \AA}^2\cdot\text{molecule}^{-1}\cdot\text{min}^{-1}$  up to the collapse pressure. Surface pressure and film area were continuously measured and recorded with a KSV Minitrough equipment (KSV, Helsinki, Finland). The phase transitions points were estimated by the third derivate method.<sup>30</sup> To compare the phase state of the investigated films and to obtain information on molecular ordering in monolayer, the compressibility modulus ( $C_s^{-1}$ ) was calculated from the isotherm data as<sup>30</sup>

$$C_s^{-1} = -\text{MMA} \left( \frac{\partial \pi}{\partial \text{MMA}} \right)_T \quad (1)$$

where MMA is the mean molecular area of a lipid monolayer at a constant temperature ( $T$ ).

**2.4. Brewster Angle Microscopy of Lipid Monolayers.** The monolayers were observed while compressed using Brewster angle microscopy (BAM). A KSV Minitrough equipment (KSV, Helsinki, Finland) was placed in a Nanofilm EP3 Imaging Elipsometer (Accurion, Gottingen, Germany) used in the BAM mode. Zero reflection was set with a polarized laser ( $\lambda = 532 \text{ nm}$ ) incident on the bare TBS surface at the experimentally calibrated Brewster angle ( $\approx 53.1^\circ$ ). After monolayer formation and compression, the reflected light was collected with a 20x objective. The quantification of the extent of area covered by Le phase and domain borders was calculated by an interactive image processing routine written in MatLab 7.9.0 developed by the Toxins and Liposomes lab at CEP. For these determinations, at least 15 pictures were analyzed from two independent experiments of each composition.

**2.5. Determination of Viscosity of the Le and Lo Lipid Phases in Lipid Monolayers.** Lipid monolayers were formed by depositing the chloroform:methanol (2:1, v:v) lipid solution containing 1 mol % of Rho-PE at the air/TBS interface of a small trough until reaching the surface pressure of  $20 \text{ mN}\cdot\text{m}^{-1}$  measured with a  $\mu$ Trough-S system (Kibron, Helsinki, Finland). The trough was placed on the stage of an Axiovert-200 fluorescence microscope (Zeiss, Germany), and the images were obtained with a long distance 20x objective and a high sensitive EMCCD camera (IxonEM+ model DU-897, Andor Technology). The observations were carried out at  $23 \pm 1^\circ\text{C}$ . The diffusion coefficient of Lo domains in a Le environment at  $20 \text{ mN}\cdot\text{m}^{-1}$  was obtained by tracking the movement of the Lo domains. Similarly, the diffusion coefficient of Le domains inserted in a Lo phase was calculated by tracking the Le domains enclosed in a larger Lo domain. The tracked domain radii in the DOPC:SM:Chol monolayers were  $1.5 \pm 0.2 \mu\text{m}$  and  $0.7 \pm 0.2 \mu\text{m}$  for Lo and Le phases, respectively, while in the case of DOPC:SM:Erg monolayers they were  $1.0 \pm 0.2 \mu\text{m}$  and  $0.7 \pm 0.2 \mu\text{m}$  for Lo and Le phases, respectively. Since convection may be reduced but not completely abolished, the domain movement was calculated from the trajectories of two domains that suffered a similar convection drag (it was assumed that, at a close enough distance,  $\leq 20 \mu\text{m}$ , the domains suffered the same drag). Therefore, the relative position of domains selected in pairs was followed in movies obtained using fluorescence microscopy with a rate of 1 frame/0.08 s. The videos, originally in gray scale, were binarized, and the center of mass of each domain was localized using an image processing routine written in MatLab 7.9.0 developed by the Toxins and Liposomes Laboratory at CEP. The position of the domain center was tracked in each frame using the plugin software “Manual tracking” associated with the ImageJ 1.43u program (NIH, USA). The relative mean square displacement of a domain relative to another one (MSD) was calculated and plotted as a function of the time elapsed between frames ( $\delta t$ ) and the diffusion coefficient ( $D$ ) can be obtained from<sup>31,32</sup>

$$\text{MSD} = 8D\delta t \quad (2)$$

The dependence of  $D$  on the surface viscosity can be expressed as follows:

$$D = \frac{kT}{r_{\text{dom}} 4\pi\eta\Lambda_T(\varepsilon)} \quad (3)$$

Here,  $k$  is the Boltzmann constant,  $T$  stands for temperature,  $r_{\text{dom}}$  is the domain radius,  $\eta$  is the viscosity of the subphase ( $0.001 \text{ Ns/m}^2$ ), and  $\Lambda_T$  is the reduced translational drag coefficient, which depends on  $\varepsilon = r_{\text{dom}} \eta / \eta_m$  as indicated in the work of Hughes et al.<sup>33</sup> Using eq 3,  $\Lambda_T$  can be obtained, and thereby  $\varepsilon$  and the membrane viscosity sensed by the tracked domain can be determined, as described in the work of Wilke et al.<sup>31,32</sup>

**2.6. Conjugation of St I with Alexa Dye.** Conjugation of St I with the dye was performed in 100 mM  $\text{NaHCO}_3$  (pH 8.3). St I was incubated with the amine-reactive dye Alexa Fluor 488 carboxylic acid succinimidyl ester, which was dissolved in dimethyl sulfoxide (DMSO) and immediately added to the protein solution. The final DMSO dilution in the examined sample was 1:10. The reaction mixture was incubated for 1 h in the dark, at room temperature under constant stirring. The conjugated protein was separated from the unreacted dye by filtering through Amicom Ultra 0.5 10K filter (Millipore Corp., USA). The obtained conjugate evidenced an average label of 2:1 Alexa/St I (calculated from absorbance measurements). The St I-Alexa conjugate was 1:5 diluted with unlabeled toxin and stored in the dark at 4 °C until use. The activity of the toxin mixture was similar to the unlabeled toxin, as showed in the hemolytic assay (data not shown) as described elsewhere.<sup>34</sup>

**2.7. Visualization of St I-Alexa Conjugate Bound to Supported Monolayers.** Lipid monolayers were formed by deposition of the chloroform:methanol (2:1, v:v) lipid solution including 1 mol % of Rho-PE at the air/TBS interface of a circular compartment until reaching the surface pressure of  $20 \text{ mN}\cdot\text{m}^{-1}$  in a  $\mu\text{Trough-S}$  system (Kibron, Helsinki, Finland). After solvent evaporation, the 1:5 mixture of St I-Alexa/St I unlabeled was injected into the subphase to reach a final concentration of  $0.8 \mu\text{M}$ . When a stable signal was obtained, the Langmuir-Schaefer technique was performed as previously described using alkylated glass as a solid support.<sup>35</sup> Coverslips were previously alkylated with octadecyltrichlorosilane to self-assemble a covalently linked monolayer of octadecylsilane in order to obtain a hydrophobic surface.<sup>35,36</sup>

Fluorescence visualization of the transferred monolayers was carried out on a Zeiss Axioplan microscope (Carl Zeiss, Oberkochen, Germany) using a mercury lamp (HBO 50), a 63X water-LD objective, and a CCD Olympus MX10 camera (Olympus Corp. USA). The rhodamine and fluoresceine filters were used to observe the Le marker Rho-PE and St I-Alexa localization, respectively. The absence of fluorescence bleeding was checked with single-marked (Rho-PE) films observed through both filters. The images were taken using the acquisition software without activating the autocontrast mode in order to keep a quantitative St I-Alexa gray level relationship. Background fluorescence was obtained from control experiments. The Le/Lo partition ratio of St I-Alexa in monolayers was calculated from the ratio of gray level in the two coexistent phases in each picture after subtracting the background signal. The error caused due to quenching of the film fluorescence was eliminated by calculating the Le/Lo fluorescence ratio for each image independently, and considering that the fluorescence quenching would equally affect both phases. At least eight measurements accomplished in two independent samples were imaged for each monolayer composition. All the experiments were carried out at  $23 \pm 2$  °C.

**2.8. Leakage Studies of CF-Containing Small Unilamellar Vesicles (SUVs).** The appropriate amounts of lipids dissolved in chloroform:methanol (2:1, v:v) were mixed and evaporated thoroughly at 50 °C. Multilamellar vesicles (MLVs) were prepared by hydration of the dried lipid mixture with 80 mM of CF (pH 7.0). SUVs were prepared through sonication of MLVs using an ultrasonicator (Branson 450, Danbury, USA) equipped with a titanium tip and subjected to 15 cycles of 1 min sonication between resting intervals of 1 min. Titanium particles released from the tip were removed by further centrifugation at  $10\,000g$  for 10 min. To remove untrapped CF, the vesicles were filtered through mini-columns

(Pierce, Rockford, USA) loaded with Sephadex G-50 (medium) pre-equilibrated with TBS.

SUVs permeabilization was assessed using a FLUOstar OPTIMA microplate reader (BMG Labtech, Offenburg, Germany) by measuring the fluorescence ( $\lambda_{\text{exc}} = 490 \text{ nm}$  and  $\lambda_{\text{em}} = 520 \text{ nm}$ ) of CF released. St I was 2-fold serially diluted in the well microplate in a final volume of 100  $\mu\text{L}$  of TBS, and the permeabilization was started by adding the same volume of SUVs (10  $\mu\text{M}$  of final lipid concentration). After mixing vesicles and St I, the release of CF produced an increase in fluorescence ( $f$ ) due to the dequenching of the dye into the external medium, which was resolved in time. Spontaneous (toxin-free) leakage of dye was negligible under these conditions. Maximum release was always obtained by adding 1 mM Triton X-100 (final concentration) and provided the fluorescence value  $f_{\text{max}}$ . The fraction of fluorophore release ( $f$ ) was calculated as follows:

$$f = \frac{f_t - f_0}{f_{\text{max}} - f_0} \quad (4)$$

where  $f_0$  and  $f_t$  represent the value of fluorescence before and at time  $t$  after St I addition, respectively.

The parameter  $C_{50\%}$  was calculated by fitting dose-dependence curves of permeabilization induced by St I to a Hill sigmoid using Origin 8.0, Microcal Inc. (USA).

**2.9. Optical and Fluorescence Microscopy of Giant Unilamellar Vesicles (GUVs).** GUVs were prepared by the electroformation procedure.<sup>37</sup> Here, 20  $\mu\text{L}$  of 2 mg/mL lipid stock chloroform solution including up to 0.2 mol % of Rho-PE were spread on the surfaces of two conductive glass slides coated with indium tin oxide. The glass slides were placed with their conductive sides facing each other and separated by a 2 mm thick Teflon frame. The chamber was filled with 0.2 M sucrose solution and placed inside an oven at  $\sim 55$  °C. The glass plates were connected to a function generator and an alternating voltage of 2 V with a 10 Hz frequency was applied for 2 h. GUVs were observed in the following day to guarantee that they have reached the thermodynamic equilibrium. The vesicles were then diluted in 0.2 M glucose containing St I (21 nM final concentration) and immediately observed in the optical microscopy. The osmolality of the sucrose and glucose solutions were measured with a cryoscopic osmometer Osmomat 030 (Gonotec, Germany) and matched to avoid differences in osmotic pressure. All measurements were done at  $23 \pm 2$  °C. Vesicles were observed in the phase contrast mode with an inverted microscope Axiovert 200 (Carl Zeiss, Jena, Germany) equipped with a Plan Neo-Fluar 63X Ph2 objective (NA 0.75) and A-plan 10X Ph1 (NA 0.25). Images were recorded with an AxioCam HSM digital camera (Carl Zeiss, Jena, Germany). Visualization of the effect elicited by St I on GUVs was performed by optical contrast fading and quantified by taking into account the changes in the brightness intensity through the ImageJ 1.43u program (NIH, USA). The pore forming activity on GUVs was estimated as the relative amount of GUVs that showed halo intensity after St I treatment as a function of time. The results represent the average of at least 10 GUVs in three independent experiments. A filter with excitation at 538–563 nm and emission at 570–640 nm (Zeiss filter set 43 HE) and a mercury lamp HXP-R 120 W were used for observing Rho-PE-labeled vesicles in the fluorescence mode.

**2.10. Statistical Analysis.** Statistical analysis was performed using STATISTICA data analysis software system, version 8.0 (StatSoft, Inc., Tulsa, USA). The Kolmogorov–Smirnov test was used to verify normal distribution of data, and the Hartley test and Levene test were used to determine the homogeneity of variance. Data with normal distribution and homogeneity of variance were analyzed with the Student  $t$  parametric test to assess statistical significance between the means of two independent groups or one-way variance analysis (ANOVA) of simple classification when more than two groups were compared, with Tukey as a *post hoc* test to assess statistical significant differences between the mean of independent group means.



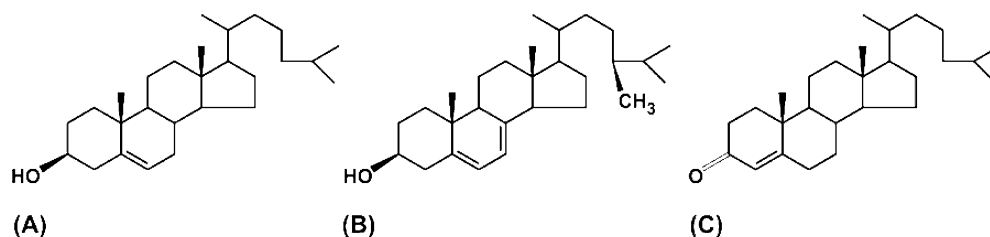


**Figure 1.** Chemical structure of (A) cholesterol, (B) ergosterol, and (C) cholestenone.

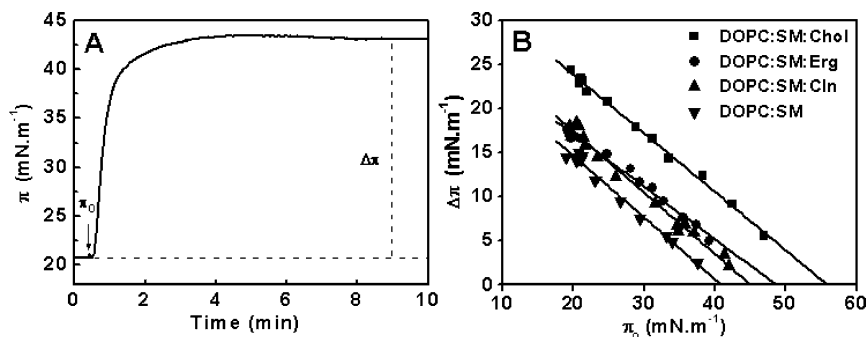


**Figure 2.** Interaction of St I with lipid monolayers. (A) Time profile of the increase in  $\pi$  after St I addition to DOPC:SM:Chol (1:1:1) monolayer. The arrow indicates the addition of St I (final concentration  $0.8 \mu\text{M}$ ). (B) Critical pressure induced by St I on monolayers of different lipid composition. Line represents the best linear fit of  $\Delta\pi$  as a function of  $\pi_0$ . Experiments were carried out under constant stirring.  $T = 23 \pm 2^\circ\text{C}$ .

**Table 1.** Interaction of St I with Lipid Monolayers and Their Characterization

composition	parameters derived from St I-monolayer binding			monolayer characterization			
	$\Delta\pi$ ( $\text{mN}\cdot\text{m}^{-1}$ ) <sup>a</sup>	$\pi_c$ ( $\text{mN}\cdot\text{m}^{-1}$ ) <sup>b</sup>	$\text{Cs}^{-1}$ ( $\text{mN}\cdot\text{m}^{-1}$ ) <sup>c</sup>	phase state <sup>d</sup>	Le phase area (%) <sup>e</sup>	domain perimeter ( $10^4$ ) ( $\mu\text{m}$ ) <sup>f</sup>	Le/Lo St I partition ratio <sup>g</sup>
DOPC:SM:Chol	$22.4 \pm 0.4$ <sup>a</sup>	$55.8 \pm 0.6$	$70 \pm 2$	Lo/Le	$58.4 \pm 3.0$ <sup>n</sup>	$7.0 \pm 0.6$ <sup>y</sup>	$1.04 \pm 0.01$
DOPC:SM:Erg	$16.1 \pm 0.6$ <sup>b</sup>	$48.5 \pm 0.8$	$89 \pm 2$	Lo/Le	$66.0 \pm 3.2$ <sup>m</sup>	$7.7 \pm 0.4$ <sup>x</sup>	$1.19 \pm 0.04$
DOPC:SM:Cln	$16.6 \pm 0.9$ <sup>b</sup>	$44.8 \pm 0.6$	$44 \pm 1$	Le	-	-	-
DOPC:SM	$14.0 \pm 0.3$ <sup>b</sup>	$40.7 \pm 0.6$	$54 \pm 6$	Le	-	-	-

<sup>a</sup> $\Delta\pi$ :  $\pi$  increase of the lipid monolayer at  $\pi_0 = 20 \text{ mN}\cdot\text{m}^{-1}$  due to St I binding. Mean  $\pm$  standard error of the mean (SEM) from at least three independent experiments are shown. Statistical analysis was performed with one-way ANOVA with Tukey as a *post hoc* test. Different letters indicate independent groups with significant differences among them ( $p < 0.05$ ). <sup>b</sup> $\pi_c$ : pressure that must be applied to avoid incorporation of St I into the monolayer. This parameter indicates the affinity of St I for the lipid ensemble and is calculated by extrapolating regression lines from plots of  $\Delta\pi$  versus  $\pi_0$  (Figure 2) ( $r^2 > 0.97$ ). <sup>c</sup> $\text{Cs}^{-1}$ : compressibility modulus of lipid monolayers at  $20 \text{ mN}\cdot\text{m}^{-1}$ . Mean  $\pm$  SEM from at least two independent experiments are shown. <sup>d</sup>Phase coexistence determined by BAM (Figure 4). <sup>e</sup>Le phase area (%): Percentage of image area occupied by the Le phase. Mean  $\pm$  SD from at least 15 BAM image frames obtained from two independent experiments are shown. Statistical analysis was performed with the Student *t* parametric test. Different letters indicate independent groups with significant differences among them ( $p < 0.05$ ). <sup>f</sup>Domain perimeter: quantitative measure of domain edges. Mean  $\pm$  SD from at least 15 BAM image frames obtained from two independent experiments are shown. Statistical analysis was performed with the Student *t* parametric test. Different letters indicate independent groups with significant differences among them ( $p < 0.05$ ). <sup>g</sup>The partition ratio was calculated from the gray level measurement of different phases of each picture. Mean  $\pm$  SD from at least eight measurements accomplished in two independent experiments are shown.

### 3. RESULTS

**3.1. Interaction of St I with Lipid Monolayers.** In order to gain insight into the influence of coexisting lipid domains on St I interaction with model membranes, we prepared monolayers composed of ternary mixtures of DOPC:SM:sterol (1:1:1) including Chol, Erg, or Cln (Figure 1) and the binary composition DOPC:SM (1:1) as a control, which is a typical mixture used to characterize binding and pore forming ability of actinoporins.<sup>14,18,25</sup> At the lipid proportion chosen, the ternary mixture PC:SM:Chol shows the coexistence of two immiscible liquid phases based on phase diagrams reported for bilayers<sup>24,38</sup> and monolayers.<sup>39,40</sup> This lipid composition represents a profusely used model for studying the properties of membrane containing Chol-enriched Lo domains.<sup>24,38,39</sup> On the other hand, the Erg-containing mixture also forms Lo domains, while

Cln has been classified as an inhibitor of Lo domain formation.<sup>26</sup>

When a monolayer of DOPC:SM:Chol was structured at the air/water interface at constant area, the injection of St I ( $0.8 \mu\text{M}$ ) induced an increase in surface pressure ( $\Delta\pi$ ), which became stabilized after  $\sim 4$  min (Figure 2A). This parameter is commonly employed to characterize the ability of the protein to interact with organized lipids.<sup>19,25,41</sup> At  $20 \text{ mN}\cdot\text{m}^{-1}$ , the increase in surface pressure promoted by St I in lipid monolayers was maximum for DOPC:SM:Chol and significantly different from that of DOPC:SM:Erg, DOPC:SM:Cln, and the binary mixture. The Erg- and Cln-containing mixtures and the binary film did not show significant differences in  $\Delta\pi$  increase among them upon addition of St I (Table 1). The increase in  $\pi_0$  provoked the reduction of  $\Delta\pi$  elicited by the

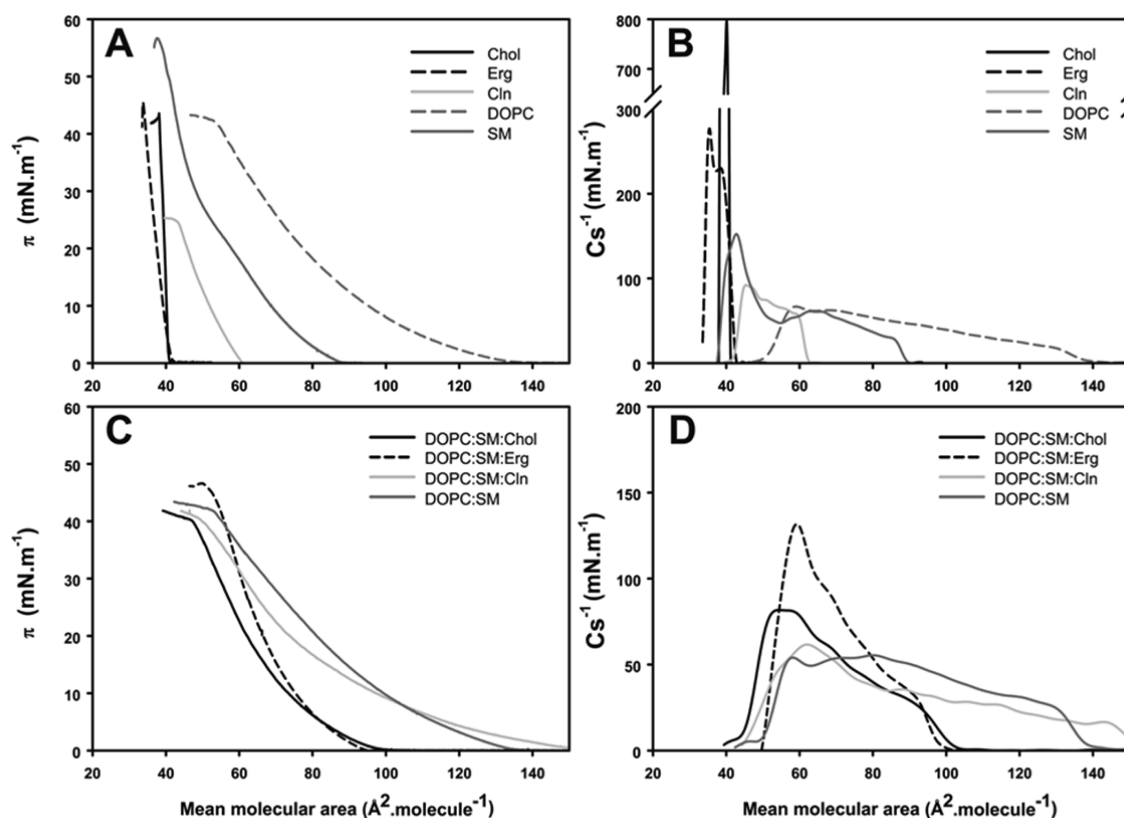


**Figure 3.** Surface behavior of lipid monolayers of different composition at the air–water interface. Compression isotherm (A and C) and surface compressibility modulus ( $C_s^{-1}$ ) (B and D) of monolayers composed by a single lipid (A and B) or lipid mixtures (C and D) as indicated. The  $C_s^{-1}$  was estimated according to eq 1. The figure shows representative curves from a set of three independent experiments.  $T = 23 \pm 2$  °C.

toxin since the initial tighter lipid packing prevents protein insertion in the lipid monolayer (Figure 2B). An appropriate parameter for the characterization of the interaction of the toxin and the monolayer is the critical pressure ( $\pi_c$ ), obtained by extrapolating to zero  $\Delta\pi$  as a function of  $\pi_0$ . This parameter corresponds to the minimum pressure that must be applied to avoid incorporation of the toxin into a monolayer and is directly correlated with its affinity for the film.<sup>41–43</sup> In all lipid monolayers,  $\pi_c$  was larger than 35  $\text{mN}\cdot\text{m}^{-1}$  (Table 1), a value that has been associated with the lateral pressure of a typical biological membrane.<sup>41</sup> Even though this is only a mean value since the pressure in membranes fluctuates,<sup>42</sup> it has been proposed that when  $\pi_c$  is higher than this critical limit, the protein not only associates to the monolayer but also penetrates it.<sup>43</sup> Moreover,  $\pi_c$  of St I strongly depended on the composition of the monolayer and varied in the order DOPC:SM:Chol > DOPC:SM:Erg > DOPC:SM:Cln > DOPC:SM (Figure 2B and Table 1). In line with differences in  $\Delta\pi$  values at 20  $\text{mN}\cdot\text{m}^{-1}$ , the  $\pi_c$  corresponding to the Chol-containing mixture showed the highest value among the compositions examined.

To assess whether the differences in St I binding to monolayers were related to the structural and rheological properties of the lipid model systems, we characterized them by combining compression isotherms, BAM explorations, and single particle tracking experiments. Figure 3A shows the surface behavior of the single-component monolayers of the lipids used in this study. DOPC formed monolayers in Le phase, while monolayers composed of SM showed an Le/Lc phase transition at  $\sim 25$   $\text{mN}\cdot\text{m}^{-1}$  (Figure 3A), in correspondence to previous reports.<sup>44–46</sup> However, the Le nature of both

monolayers is evidenced by low  $C_s^{-1}$  values, with 150  $\text{mN}\cdot\text{m}^{-1}$  (Figure 3B) being the cutoff accepted to delineate the existence of Le or Lc phase for most PC and SM.<sup>45,46</sup> On the other hand, Chol and Erg showed isotherm curves that respond sharply to compression (Figure 3A). This is reflected by very high  $C_s^{-1}$  values, more prominent for Chol than for Erg (Figure 3B) as previously described.<sup>47</sup> By contrast, pure Cln monolayer analysis reveals that the isotherm curve is less sharp with low compressibility modulus ( $<100$   $\text{mN}\cdot\text{m}^{-1}$ ) and the collapse pressure is notably lower ( $\sim 25$   $\text{mN}\cdot\text{m}^{-1}$ ) than the other lipid components ( $\sim 40$ – $55$   $\text{mN}\cdot\text{m}^{-1}$ , Figure 3A). This description, along with microscopy evidence, led to the classification of Chol and Erg as “membrane-active” and Cln as a “membrane-inactive” sterol.<sup>47</sup>

From the compression isotherm data of mixed monolayers (Figure 3C) we could assign a Le character to all analyzed mixed lipid films based on the smooth behavior of the curves. However, the analysis of the  $C_s^{-1}$  versus MMA revealed that DOPC:SM:Erg and DOPC:SM:Chol monolayers showed the highest values of  $C_s^{-1}$  (80 and 130  $\text{mN}\cdot\text{m}^{-1}$ , respectively), compared to those of DOPC:SM:Cln and DOPC:SM monolayers (50–60  $\text{mN}\cdot\text{m}^{-1}$ , see Figure 3D). The  $C_s^{-1}$  values at 20  $\text{mN}\cdot\text{m}^{-1}$ , reflected these differences among lipid mixtures (Table 1). It is worth noting that the compressibility is a macroscopic property that accounts mainly for the phase state of the continuous phase on a heterogeneous film,<sup>48</sup> which in the monolayers studied is the Le phase. Thus, the Le phase seems to be less compressible in monolayers comprising Erg and Chol than in the monolayer including Cln and the binary mixture.

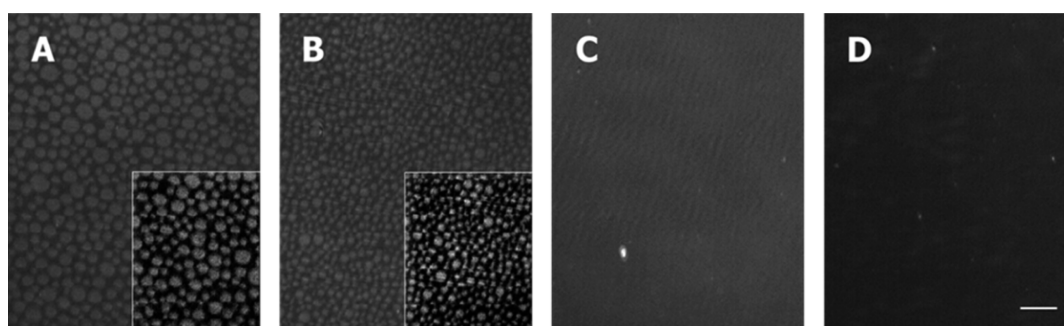


**Figure 4.** Visualization of lipid monolayers by BAM. Images were taken at  $20 \text{ mN}\cdot\text{m}^{-1}$ . Lipid composition: (A) DOPC:SM:Chol (1:1:1), (B) DOPC:SM:Erg (1:1:1), (C) DOPC:SM:Cln (1:1:1), and (D) DOPC:SM (1:1). For better visualization, the lower 0–90 gray level range (from the 0 to 255 original scale) was selected in order to keep the gray level–film thickness ratio. Images are representative of two independent experiments. The scale bar in panel D represents  $100 \mu\text{m}$  and is equivalent for all images. The insets to A and B show a piece of both images enhanced by a bandpass filter.  $T = 23 \pm 2 \text{ }^{\circ}\text{C}$ .

The monolayers were observed by BAM in order to assess the microstructure of the films. The gray level of BAM images depends on both the refractive index of the film and the monolayer thickness.<sup>40</sup> Monolayers composed of DOPC:SM:Chol and DOPC:SM:Erg exhibited phase coexistence in the whole range of surface pressure analyzed as shown at  $20 \text{ mN}\cdot\text{m}^{-1}$  (Figure 4A and 4B, respectively). Lo domains, which are usually thicker and show higher refractive index, appear as light gray areas surrounded by a dark gray Le phase. An uniform dark gray phase with Le character was observed in DOPC:SM:Cln and DOPC:SM monolayers (Figure 4C,D, respectively) at all pressures. These findings are in agreement with previous results that classified Chol and Erg as promoters of Lo/Le phase coexistence, while Cln is considered an inhibitor of Lo domain formation.<sup>26,28</sup> The quantitative analysis of BAM images such as those shown in Figure 4A,B revealed that the Le phase represents 58% and 66% of the monolayer area for the DOPC:SM:Chol and DOPC:SM:Erg mixtures, respectively (Table 1). Regarding the film texture, the Chol-containing films showed a lesser number of Lo domains than those of the mixture DOPC:SM:Erg (Figure 4A,B); hence the Erg-containing monolayer showed larger amount of total domain edges (Table 1).

We further studied the effect of sterol structure on the lateral diffusion of lipid domains in those monolayers showing phase coexistence (monolayer containing Chol or Erg) by fluorescence microscopy (FM). To this end, we included 1 mol % of Rho-PE into both DOPC:SM:Chol and DOPC:SM:Erg monolayers. In the presence of two physically different phases, this probe has a preferential partition into the less ordered phase, thus probe exclusion can be considered a marker of Lo domains. In agreement with BAM experiments, DOPC:SM:Chol and DOPC:SM:Erg films showed two coexisting phases: the lighter phase enriched in the lipidic probe (Le phase) and the darker one (Lo phase, Figure 5A,B, respectively). The shear viscosity of each phase was tested by the tracking of single lipid domains as detailed in Section 2.5. Figure 5C shows the viscosity of the film for both Le and Lo phases in DOPC:SM:Chol and DOPC:SM:Erg monolayers at  $20 \text{ mN}\cdot\text{m}^{-1}$ . In DOPC:SM:Chol monolayers the Lo domains reached a  $\eta_m$  value about 2–3 fold higher than that corresponding to the Le phase, while for the DOPC:SM:Erg film both phases showed similar  $\eta_m$  values, not differing significantly from the Lo phase of the DOPC:SM:Chol monolayer. Remarkably, the Le phase in the DOPC:SM:Erg monolayer had a viscosity value

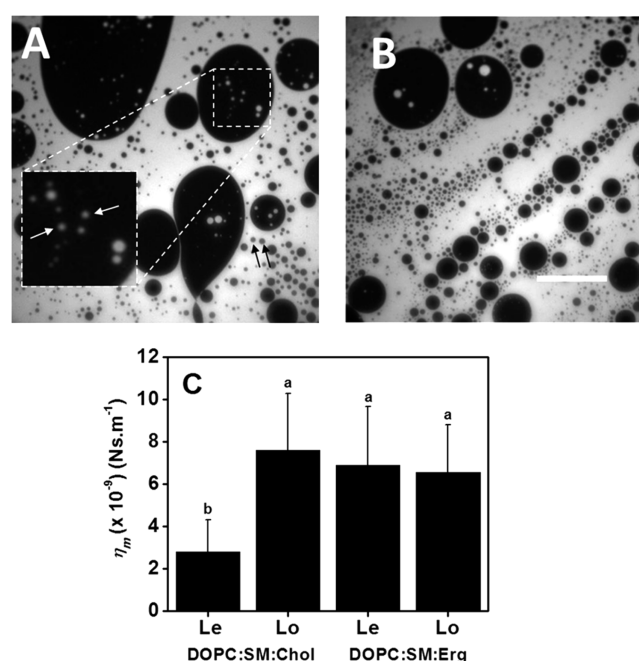


**Figure 5.** Determination of viscosity of the Le and Lo lipid phases in lipid monolayers. Representative fluorescence microscopy images of monolayers at a surface pressure of  $20 \text{ mN}\cdot\text{m}^{-1}$ : (A) DOPC:SM:Chol (1:1:1) and (B) DOPC:SM:Erg (1:1:1), containing in both cases 1 mol % Rho-PE. The inset in panel A represents a 2X amplification of the selected area. The arrows show examples of domains analyzed in the single particle tracking experiment.  $\eta_m$  of Lo and Le phases are shown in panel C.  $\eta_m$  represents the monolayer viscosity determined as described in eq 3. Bars show the mean value of  $\eta_m$  and the standard deviation from 10 to 15 individual single particle tracking experiments. Lo and Le stand for the liquid-expanded and liquid-ordered phases, respectively. Statistical analysis was performed with one-way ANOVA with Tukey as a *post hoc* test. Different letters indicate independent groups with significant differences among them ( $p < 0.05$ ). The scale bar in B represents  $40 \mu\text{m}$  and is equivalent for both images.  $T = 23 \pm 2 \text{ }^{\circ}\text{C}$ .

about 2–3 fold higher than that of the Le phase in the DOPC:SM:Chol monolayer.

Understanding the enhancing effect of sterols on St I binding to lipid monolayers is important to identify the preferential localization of St I in films with Le/Lo coexisting phase. For this purpose, we labeled St I with the fluorescent probe Alexa 488 and mixed it with unlabeled toxin in a molar



proportion of 1:5 (St I-Alexa: unlabeled St I). The selection of the appropriate fluorescence filter allowed the visualization by FM of either the lipid monolayer or St I-Alexa in the same preparation. The double labeled films of DOPC:SM:Chol monolayers showed that St I-Alexa was identified in both lipid phases (Figure 6A,C). The analysis of the fluorescence intensity

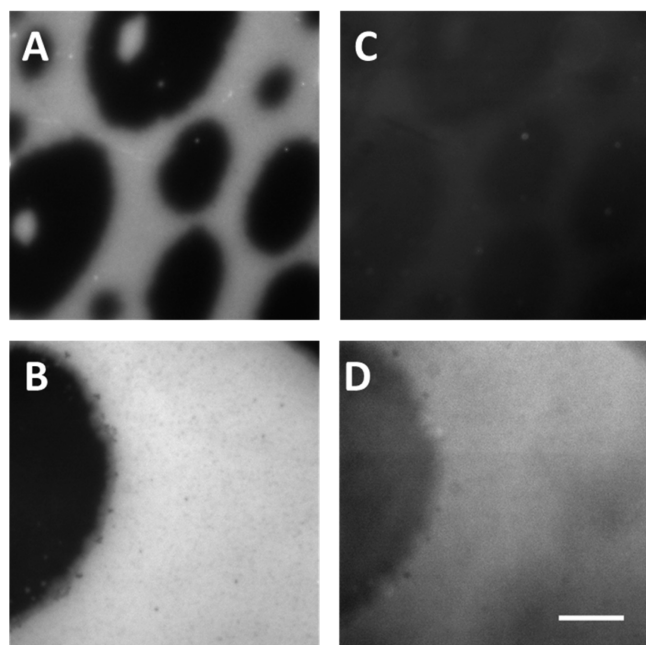


**Figure 6.** Le/Lo phase coexistence epifluorescence images of Rho-PE labeled lipid monolayers containing fluorescently labeled St I. Left column (A and B) shows images of monolayers at 20 mN·m<sup>-1</sup> viewed through a rhodamine filter, and in the right column (C and D) the same frames are imaged through an Alexa 488 filter. Lipid composition: (A and C) DOPC:SM:Chol (1:1:1) and (B and D) DOPC:SM:Erg (1:1:1) containing in both cases 1 mol % Rho-PE. St I-Alexa concentration: 0.8 μM. The scale bar in (D) represents 20 μm and corresponds to the size of all images. *T* = 23 ± 2 °C.

of Le and Lo lipid phases revealed no relative preference of St I for any phase as reflected for Le/Lo partition ratio (Table 1). However, in DOPC:SM:Erg monolayer, St I-Alexa had a preferential adsorption to the continuous Le phase (Figure 6D and Table 1).

**3.2. Vesicle Permeabilization by St I.** To evaluate whether the affinity of St I in the presence of different sterols correlated with the protein activity, we examined the pore forming ability of the toxin using SUVs and GUVs of the same lipid compositions described in the monolayer studies. From CF release assays in SUVs, the final extent of the St I permeabilization activity at 10 min was plotted as a function of toxin/lipid molar ratio (Figure 7). In order to compare the relative activity of St I, the parameter *C*<sub>50%</sub> was determined by fitting the experimental data to a Hill sigmoid (Figure 7 and Table 2). Liposomes containing Chol were around ~12-fold more susceptible to St I permeabilization than PC:SM vesicles, and almost twice more susceptible than those comprising Erg or Cln. In turn, St I showed similar pore-forming ability in Erg or Cln-containing vesicles, and it was ~5-fold higher than in PC:SM vesicles. Therefore, the pore-formation activity of St I was enhanced by the presence of sterols in membrane in the sequence Chol > Erg ~ Cln.

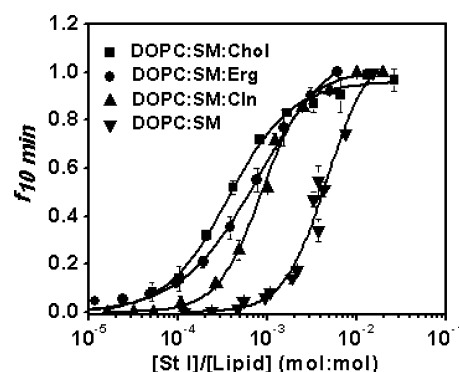


**Figure 7.** Pore-forming activity of St I on SUVs of different lipid composition. *f*<sub>10 min</sub> represents the value of fluorescence at time 10 min after St I addition. Points are the mean value, and bars indicate the standard deviation from a set of three independent experiments. Solid line is the best fit of experimental data to a Hill function (*R*<sup>2</sup> > 0.96) using Origin 8.0, Microcal Inc. (USA). Lipid composition: (■) DOPC:SM:Chol (1:1:1), (●) DOPC:SM:Erg (1:1:1), (▲) DOPC:SM:Cln (1:1:1), and (▼) DOPC:SM (1:1:1). Buffer solution: TBS 300 mM NaCl, pH 7.0. *T*: 23 ± 2 °C.

**Table 2.** Pore-Forming Activity of St I

composition	SUV permeabilization	GUV permeabilization	GUV phase state <sup>c</sup>
	<i>C</i> <sub>50%</sub> (× 10 <sup>-4</sup> ) (mol:mol) <sup>a</sup>	relative halo intensity <sub>20 min</sub> (%) <sup>b</sup>	
DOPC:SM:Chol	3.7 ± 0.1 <sup>c</sup>	29 ± 15 <sup>z</sup>	Lo/Ld
DOPC:SM:Erg	8.4 ± 2.7 <sup>b</sup>	68 ± 12 <sup>y</sup>	Lo/Ld
DOPC:SM:Cln	8.6 ± 0.5 <sup>b</sup>	80 ± 10 <sup>xy</sup>	Ld
DOPC:SM	46.4 ± 2.2 <sup>a</sup>	90 ± 5 <sup>x</sup>	Ld

<sup>a</sup>*C*<sub>50%</sub>: toxin/lipid molar ratio necessary to promote the release of 50% of CF entrapped in SUV. The parameters were calculated by fitting dose-dependence curves of permeabilization induced by St I to a Hill sigmoid (*R*<sup>2</sup> > 0.96) using Origin 8.0, Microcal Inc. (USA). Mean ± SD from two independent experiments are shown. Statistical analysis was performed with one-way ANOVA with Tukey as a *post hoc* test. Different letters indicate independent groups with significant differences among them (*p* < 0.05). <sup>b</sup>Remnant vesicles showing phase contrast at 20 min after addition of St I. Mean ± SD calculated from at least 10 vesicles in three independent experiments. Statistical analysis was performed with one-way ANOVA with Tukey as a *post hoc* test. Different letters indicate independent groups with significant differences among them (*p* < 0.05). <sup>c</sup>Phase coexistence determined by fluorescence microscopy (Figure 8).

GUVs were also tested in our study since they are an excellent model of biological membranes due to its bilayer structure and dimension similar to a cell membrane. This system allowed us to assess the pore-forming activity of St I as well as further characterize the phase coexistence in this bilayer model system. GUVs were visualized by optical microscopy both in contrast phase and fluorescence modes (Figure 8). All the GUVs including those containing sterols exhibited well-defined optical contrast due to the sucrose/glucose asymmetry distribution inside and outside the vesicles, respectively (Figure 8A,C,E). Observation of GUV under the fluorescence mode revealed the presence of two micron-scaled Lo/Ld phase coexistence in DOPC:SM:Chol (Figure 8B) and DOPC:SM:Erg (Figure 8D). The darker regions in Lo state would probably be enriched in sterol and SM, whereas the brighter region in Ld phase would be rich in the unsaturated lipid DOPC. Coexisting liquid phases have been observed in a

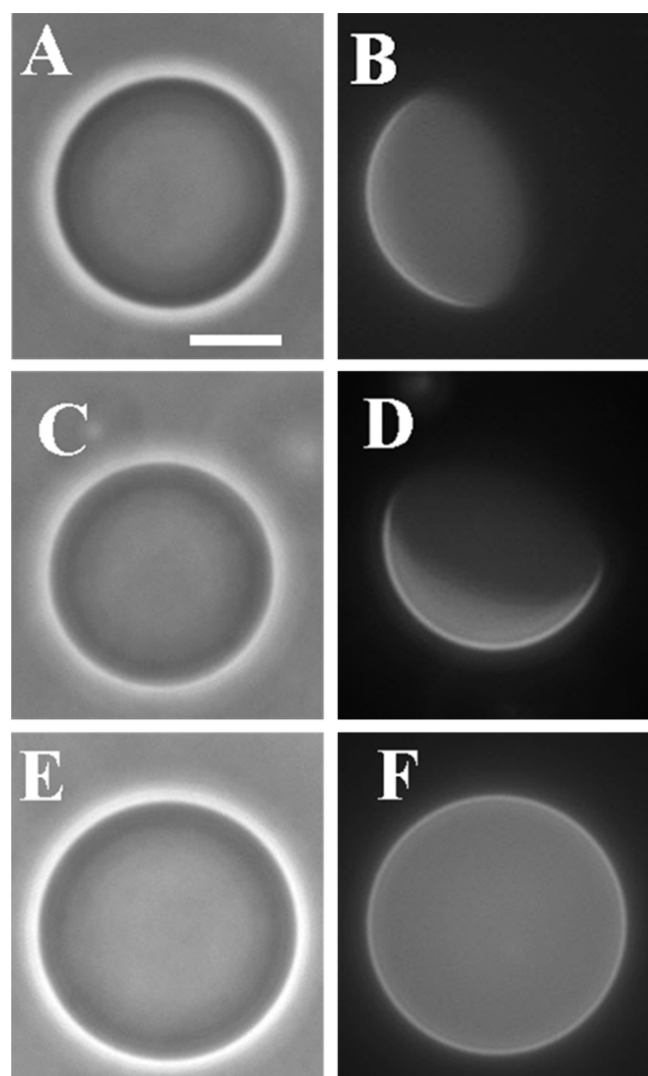


**Figure 8.** Visualization of GUV of different lipid compositions in phase contrast and fluorescence mode. DOPC:SM:Chol (1:1:1) (A and B), DOPC:SM:Erg (1:1:1) (C and D), and DOPC:SM:Cln (1:1:1) (E and F) containing in all cases 0.2 mol % of Rho-PE. The scale bar in A spans 20  $\mu\text{m}$  and corresponds to the size of all images. Left panels show phase contrast mode, and right panels show fluorescence visualization mode.  $T = 23 \pm 2$   $^{\circ}\text{C}$ .

wide variety of ternary mixtures of saturated and unsaturated phospholipids and sterols in GUVs.<sup>26,28</sup> By contrast, the ternary mixture including Cln (Figure 8F) as well as the binary mixture DOPC:SM (1:1) (data not shown) displayed an homogeneous distribution of the fluorophore. The presence of Cln in GUVs membrane did not promote visible Lo/Ld phase coexistence, similarly to what was observed by BAM in monolayers (Figure 4C), and also in agreement with its previous assignment as an inhibitor of Lo domain formation in GUVs.<sup>26</sup>

With the aim of visualizing the effect of St I, GUVs were dispersed in a protein containing-glucose solution and immediately placed in the observation chamber. As an example, Figure 9 shows how the addition of St I (21 nM) in the outer GUV suspension impacted on DOPC:SM:Chol liposomes that initially exhibited optical phase contrast (Figure 9A). Upon St I addition, such an optical contrast gradually diminished with time (Figure 9C,E) reflecting changes in the lipid bilayer permeability as a result of the inner and outer sugar solutions

exchange. This increase in membrane permeability suggests the formation of pores by the toxin. Of note, these pores must be of submicrometric dimension since we did not observe micropores during the experiment with the microscope resolution of few microns. According to previous estimates, the pore radius of St I in cells and model membranes is around 1.0 nm,<sup>49</sup> thus considering the hydrodynamic radii of both sugars glucose (0.42 nm) and sucrose (0.54 nm),<sup>50,51</sup> as well as CF ( $\sim 1.0$  nm),<sup>52</sup> all the compounds are able to pass through the toxin pore. Moreover, the formation of pores occurred without membrane disruption or solubilization after 1 h of continuous observation (data not shown).

Figure 9G displays the time course of St I permeabilization in GUVs. St I acted to a larger extent on GUVs composed of DOPC:SM:Chol, since the percentage of GUVs that keeps contrast decreased faster for this composition than for the others. Note that after 20 min of St I interaction with GUVs, those comprising Chol showed a higher exchange between the external and internal sugar solution followed by vesicles containing Erg or Cln. Of note, the St I effect on a set of GUVs containing Erg or Cln did not evince statistical differences (Table 2). For the binary mixture lacking sterol, the release under these experimental conditions was barely detectable, and almost all of vesicles remained intact.

#### 4. DISCUSSION

Chol, Erg, and Cln have a general similar structure with just small differences in particular chemical features. For instance, the main structural differences between Cln and the other two sterols is the presence of a keto group at position C3. In turn, Erg has a conjugated carbon-carbon double bond in its B steroid ring, which has two *cis* hydrogens bound to C6 and C7. Additionally, small chemical differences are also found in the alkyl side chain (Figure 1). Interestingly, such apparently subtle chemical differences impart Chol and Erg with the ability to form Lo/Ld phase coexistence while Cln does not.<sup>26,28</sup> Additionally, the behaviors upon compression of the three lipids are different, forming Cln, the more compressible, and Chol, the less compressible film. In this work, we used these sterols as an experimental approach to study the effect of membrane properties in the binding and pore forming ability of St I.

The presence of any of these sterols increases binding of St I to lipid monolayers (Figure 2 and Table 1) as previously described for Eqt II.<sup>18</sup> In general, it has been reported that the heterogeneity of membranes improves the binding and pore forming ability of actinoporins.<sup>18–23,53,54</sup> The heterogeneity of membranes can arrive not only from coexisting phases but also from different solvation degrees of polar head groups, lipid mismatch, lipid packing, and the propensity to adopt a non-lamellar phase. Here, the heterogeneity seems to be relevant beyond phase coexistence, since St I has an enhanced affinity for DOPC:SM:Cln monolayer compared to the binary mixture (Figure 2B and Table 1), although both are organized in an homogeneous Le fluid phase (Figure 4C,D and Table 1). In the same direction, Cln- and Erg-containing membranes showed no difference in St I binding to lipid monolayers at 20 mN·m<sup>−1</sup> (Table 1) despite the fact that DOPC:SM:Erg film shows Le/Lo phase coexistence (Figure 4B) while the DOPC:SM:Cln monolayer is organized in a single Le phase (Figure 4C). Accordingly, the permeabilizing activity of St I is similar in Erg- and Cln-containing vesicles (Table 2). However, in monolayers showing phase coexistence (i.e., with Chol and Erg) we have demonstrated that St I binds to a higher extent when Chol is



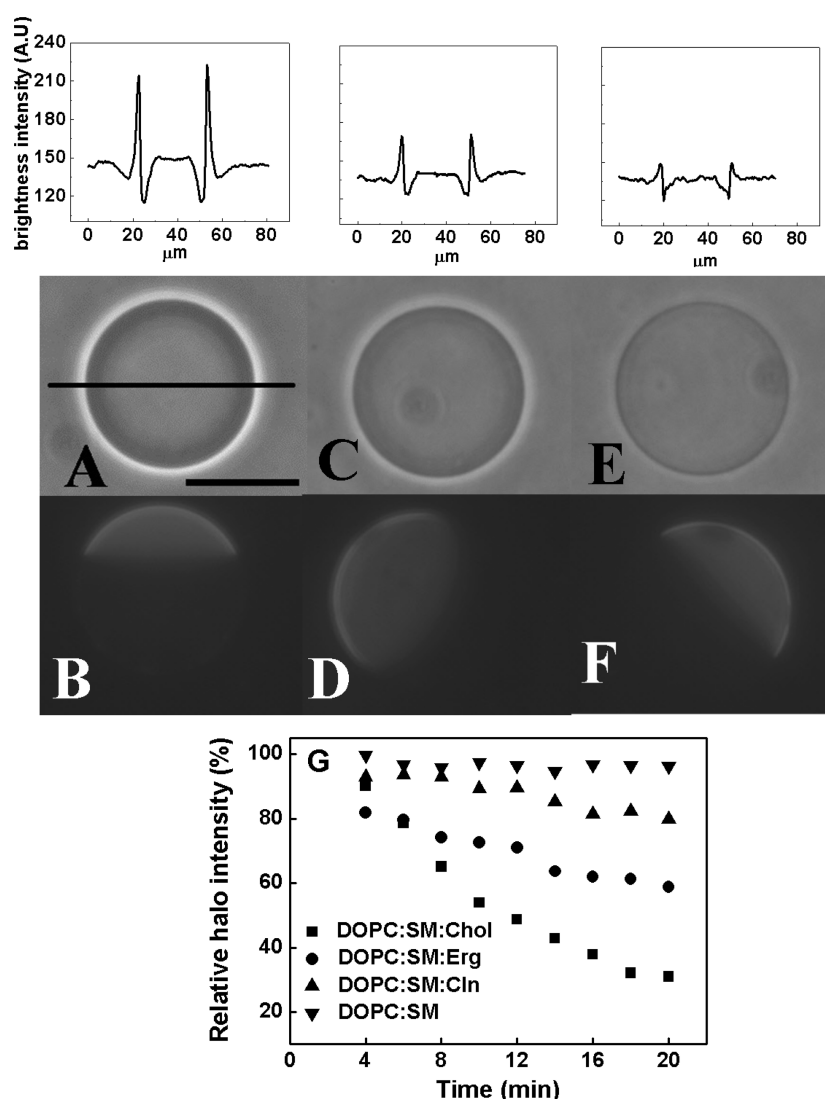


**Figure 9.** Visualization of the effect elicited by St I on GUVs of different lipid composition. Upper row: Line profiles of the phase contrast. A.U.: arbitrary units. The solid line (in lower A) indicates the transversal section selected to follow the changes in the brightness intensity. Central row: GUVs composed of DOPC:SM:Chol (1:1:1) snapshots in phase contrast and fluorescence mode immediately placed in contact with St I (A and B); after 10 min (C and D) or 20 min (E and F) of visualization. Lower row: GUV snapshots in fluorescence mode captured at the same time of snapshots showed in central row. The scale bar in A represents 20  $\mu\text{m}$ . (G) Representative kinetic curves showing the percentage of GUV of different composition that show a decrease of phase contrast after St I treatment (21 nM). Lipid composition: (■) DOPC:SM:Chol (1:1:1), (●) DOPC:SM:Erg (1:1:1), (▲) DOPC:SM:ClIn (1:1:1), and (▼) DOPC:SM (1:1).  $T = 23 \pm 2$  °C.

present, in spite of the fact that the Erg film had a higher occurrence of domain boundaries (Figure 2B and Table 1). Furthermore, a detailed inspection of the double-labeled monolayers demonstrated that Lo domain edges from DOPC:SM:Chol or DOPC:SM:Erg did not reveal an enhanced fluorescence (Figure 6), at least in the range of the detection limit of our experimental approach ( $\mu\text{m}$ ). This result is in agreement with the evidence that there is no relation between St I binding to lipid monolayers and the extent of Le/Lo linear interface (Table 1) and with our previous observation demonstrating that St I binding to PC:SM monolayers is independent of the extension of Le/Lc domain boundaries.<sup>25</sup> Our results are in contradiction with those previously reported for Eqt II, which showed its preferential partition to the Lo domain perimeter in monolayers<sup>18</sup> or GUVs.<sup>20</sup> Recent studies with Eqt II, revealed that its binding to bilayers containing Lo/Ld coexisting lipid phases is a time-dependent phenomenon.<sup>22</sup> At early stages, Eqt II was enriched at the phase boundary

between the domains, and after this initial period Eqt II concentration increased in the Ld phase, where protein preferentially accumulates. In our experimental design we transferred the film to the supporting glass when St I binding to the monolayer reached equilibrium (10–15 min). One possibility is that, under these conditions, we missed the initial stage of protein binding at the lipid interface, and we could only detected their accumulation in the Le phase (Figure 6 and Table 1). Also it cannot be disregarded that St I and Eqt II, even while being quite close actinoporins, exhibit different pore-forming activity and could behave differently in this model membrane system. Altogether, these results demonstrated that, in spite of the generally accepted viewpoint, which claims that domain edges are intrinsically favored sites for actinoporins binding and pore formation,<sup>18,20</sup> they do not seem to be the key factor governing St I functional activity (Tables 1 and 2).

In a previous work we highlighted the relevance of membrane fluidity on the incorporation of St I to membranes,

and found that the partition preferences of St I is subtly tuned by combined factors such as viscosity and SM content.<sup>25</sup> In this context, we explored the possible influence of fluidity of the sterol-containing membranes on the action of St I. St I does not appear to be sensitive to the viscosity differences between Le and Lo lipid phase, as evinced by its similar binding to both phases in the Chol-containing monolayer. This result is consistent with the evidence that Chol inclusion into PC:SM (4:1) bilayers increases binding of St II, even at molar proportions at which Chol increases membrane viscosity, indicating that membrane fluidity is not *per se* responsible for Chol enhancing effects.<sup>53</sup> Previous work developed in monolayers of dilauroylphosphatidylcholine, palmitoyl-SM and the nonoxidizable Chol analogue dihydrocholesterol (Dchol) at equimolar proportion, revealed that at 20 mM<sup>-1</sup> the Lo phase has a higher content of SM (~35 mol %) compared to ~25 mol % in the Le phase.<sup>40</sup> Taking into account the similarity between these lipids and those used in our study, it is likely that under the condition examined here, St I encounters two attractive phases in the DOPC:SM:Chol monolayer: a Lo phase with a higher proportion of SM and a Le phase also comprising SM but in a more fluid condition (Figures 5 and 6C). In addition, the presence of Chol in the Le phase of DOPC:SM:Chol (1:1:1) monolayers, which has been estimated to be around 9 mol %, <sup>40</sup> could change the physical properties of the SM headgroup, as previously suggested,<sup>53</sup> in a way that facilitates the interaction between SM and St I even though in the Le phase there is a lower SM concentration. In this scenario, the toxin might be unable to distinguish between both phases probably because they have different but very attractive properties for an optimal St I binding to membranes (high SM concentration vs membrane fluidity and SM accessibility; Table 1), as previously observed with PC:SM monolayers.<sup>25</sup> Conversely, in Erg-containing monolayers, St I discriminates both phases, even though they have similar viscosity (Figure 5C). In this context, St I shows a higher affinity for the Le phase (Figure 6D), in spite of the assumption that this phase contains lower amount of SM than the Lo. A possible explanation could be that Erg has a stronger ordering effect than Chol as has been described, turning the Lo phase in a less suitable environment for protein association. Thus, the observed increased affinity of St I to Chol-including membranes (Figure 2B and Table 1) could result from the larger representation of attractive binding sites compared with the Erg-containing one.

The three examined sterols potentiate the pore forming ability of St I, with the Chol containing vesicles being the most responsive to permeabilization (Table 2, Figures 7 and 9). Such enhanced effect can be explained taking into account the higher toxin binding to membranes containing sterols evidenced by the higher  $\pi_c$  values in the monolayer systems when compared to the binary mixture (Table 1 and Figure 2B). It is interesting to note that St I follows the same behavior in sterol-containing monolayer and bilayer systems (SUVs and GUVs). This finding allowed us to correlate binding results obtained in the monolayer system with those obtained in vesicle permeabilization assays, both in SUVs and GUVs. A recent study demonstrated that the most fluid phase is the most suitable platform for pore formation by actinoporins.<sup>22</sup> Thus, the presence of sterols in the easily deformable and less-ordered Ld phase, which may represent 20 mol % in the case of Chol (probably in close interaction with SM, 17 mol %)<sup>55</sup> appears to have important functional consequences in St I pore formation.

In fact, the St I pore-forming activity in Chol containing membranes was higher than in those containing Erg (Figure 7 and 9). In this regard, extrapolating our results obtained in the monolayer (Figure 5) to the bilayer system, it is tempting to speculate that the Ld phase in the Chol-containing vesicles behaves as more fluid and has a weaker lipid cohesion than the corresponding phase in Erg including membranes. Therefore, a higher fluidity would provide a more favorable environment for St I oligomerization and the insertion of its N-terminal membranes with Chol. Even though the phase fluidity seems not to be relevant for toxin binding to lipid monolayers, it could be important for pore formation.

In addition, the area occupied by the Le phase in DOPC:SM:Chol is smaller when compared with the Erg-containing membranes (Table 1), as was previously described in GUVs.<sup>26</sup> The confinement of the toxin to a reduced area that may contain a relatively high SM concentration (17 mol %)<sup>55</sup> and in a less ordered phase could be an efficient strategy to reduce the diffusion area to facilitate protein oligomerization and insertion into the membrane. Consequently, pore-forming activity in Chol-containing vesicles seems to become more efficient on account of both the higher fluidity of its Ld phase and the concentrating effect on St I.

It is interesting to note that Cln-containing lipidic systems show higher binding and pore forming ability than the binary mixture (Table 1 and 2). In the proteolipidic arrangement proposed for sticholysins<sup>56</sup> and Eqt II,<sup>57</sup> the bilayer distortion implies that lipids in the vicinity of the N-terminal  $\alpha$ -helix assume negative curvature in the membrane plane, characteristic of the H<sub>II</sub> structure. It has been found that Chol induces negative curvature in the bilayer and has the tendency to form inverted lipid phases such as hexagonal phase (H<sub>II</sub>).<sup>58–62</sup> This effect is mostly explained by the molecular shape of Chol which has a truncated cone shape as a result of its small headgroup compared to its hydrocarbon portion (Figure 1). In this regard, the capacity of sterols to induce H<sub>II</sub> phase has been demonstrated to correlate with the molecular area of the pure sterols in monolayers.<sup>62</sup> According to our data, Chol and Erg that showed an analogous behavior in the compression isotherms (Figure 3A) are likely to have a similar capacity to stabilize H<sub>II</sub> phase. By contrast, Cln occupies a much larger molecular area in monolayers (Figure 3A), which would probably indicate that the ring system is differently oriented at the air–water interface.<sup>62</sup> Therefore, it is possible that the presence of sterols, which favors the negative curvature of the membrane, could increase the efficiency of the pore forming ability of St I. The importance of membrane curvature for sticholysins activity was nicely demonstrated using phospholipid inducing negative curvature in the bilayer.<sup>56</sup> These authors pointed out that there is a correlation between the propensity of phospholipid to promote H<sub>II</sub> phase and the stimulation of pore formation. In agreement with this idea, the increased affinity and activity of St I in sterol-containing vesicles could be explained taking into account their capacity to generate a H<sub>II</sub> phase.

## 5. CONCLUDING REMARKS

The mechanism implicated in St I membrane interaction is quite complex, and membrane composition-organization plays a pivotal role in binding and pore-forming activity. In the current paper, our combined results give support to conclude that any of the analyzed sterols (Chol, Erg, or Cln) included into the PC:SM membranes favors membrane binding,

insertion, and pore-formation, with Chol being the strongest promoter. In this context, a remarkable consistency was found with different membrane model systems studied: monolayers and vesicles. The possible changes in the membrane biophysical properties that may be responsible of the observed results are molecular heterogeneity, fluidity, and negative curvature of the bilayer induced by the sterols. From our results, it is clear that the modulation of St I activity by sterols is a multifactorial complex phenomenon, and further research is necessary to clarify their fine-tuning action. Chol emerged as the strongest promoter of binding and pore forming ability of St I probably due to its unique capacity to combine a concentrating effect on the toxin at its smaller Ld area with the relatively higher fluid character of this phase and the ability to promote nonlamellar structures.

## AUTHOR INFORMATION

### Corresponding Author

\*Address: Centro de Estudio de Proteínas, Facultad de Biología, Universidad de La Habana, La Habana, Cuba, CP 10400. Tel.: 00537 8324830; fax: 00537 8321321; e-mail: calvarez@fbio.uh.cu.

### Notes

The authors declare no competing financial interest.

## ACKNOWLEDGMENTS

This work was supported by the Iberoamerican CYTED-BIOTOX Network (212RT0467), CONICET (PIP 112-200801-01413), SECyT from the National University of Cordoba (05/C578), FONCyT (PICT-2010-0415)-Argentina, CNPq-MES Brazil Cuba bilateral agreement and an UNU-BIOLAC fellowship given to L.P. L.P. and U.R. are grantees from IFS (5194-1 and 4616, respectively), Sweden. M.L.F. and N.W. are career investigators of CONICET, Argentina. R.I. is a recipient of a CNPq research fellowship.

## ABBREVIATIONS:

St I sticholysin I; PFTs pore-forming toxins; Chol cholesterol; PC phosphatidylcholine; Erg ergosterol; Cln cholestenone; Lo liquid ordered; Ld liquid disordered; SM sphingomyelin; Eqt II equinatoxin II; St II sticholysin II; FraC fragaceatoxin C; DOPC dioleoylphosphatidylcholine; Le liquid expanded; Rho-PE L $\alpha$ -phosphatidylethanolamine-N-lissamine rhodamine B sulfonyl-ammonium salt, chicken egg-transphosphatidylated; CF carboxyfluorescein; TBS Tris-buffered saline solution;  $\pi_0$  initial surface pressure;  $\Delta\pi$  increment in surface pressure; MSD relative mean square displacement of a domain relative to another one;  $D$  diffusion coefficient; DMSO dimethyl sulfoxide; MLVs multilamellar vesicles; SUVs small unilamellar vesicles; GUVs giant unilamellar vesicles;  $\pi_c$  critical pressure; BAM Brewster angle microscopy;  $C_s^{-1}$  compressibility modulus; FM fluorescence microscopy

## REFERENCES

- (1) Mas, R.; Menéndez, R.; Garateix, A.; García, M.; Chávez, M. Effects of a high molecular weight toxin from *Physalia physalis* on glutamate responses. *Neuroscience* **1989**, *33*, 269–273.
- (2) Loret, E. P.; Menéndez-Soto del Valle, R.; Mansuelle, P.; Sampieri, P.; Rochat, H. Positively charged amino acid residues located similarly in sea anemone and scorpion toxins. *J. Biol. Chem.* **1994**, *269*, 16785–16788.
- (3) Pazos, F.; Gómez, T.; Tejuca, M.; Alvarez, C.; Lanio, M. E. Enzymatic characteristics of a fraction with phospholipase activity

isolated from the anemone *Stichodactyla helianthus*. *Rev. Biol.* **1993**, *7*, 115–123.

(4) Romero, L.; Marcucci, S.; Marchi-Salvador, D. P., Jr.; Silva, F. P.; Fuly, A. L.; Stábeli, R. G.; da Silva, S. L.; González, J.; Monte, A. D.; Soares, A. M. Enzymatic and structural characterization of a basic phospholipase A(2) from the sea anemone *Condylactis gigantea*. *Biochimie* **2010**, *92* (8), 1063–1071.

(5) Delfin, J.; González, Y.; Díaz, J.; Chávez, M. Proteinase inhibitors from *Stichodactyla helianthus*: purification, characterization and immobilization. *Arch. Med. Res.* **1994**, *25*, 199–204.

(6) Bernheimer, A. W.; Avigad, L. S. Properties of a toxin from the sea anemone *Stoichactis helianthus*, including specific binding to sphingomyelin. *Proc. Natl. Acad. Sci. U. S. A.* **1976**, *73*, 467–471.

(7) Kem, W. R.; Dunn, B. M. Separation and characterization of four different amino acid sequence variants of a sea anemone (*Stichodactyla helianthus*) protein cytolytin. *Toxicon* **1988**, *26*, 997–1008.

(8) Anderluh, G.; Macek, P. Cytolytic peptide and protein toxins from sea anemones (*Anthozoa: Actiniaria*). *Toxicon* **2002**, *40*, 111–124.

(9) Gouaux, E. Channel-forming toxins: tales of transformation. *Curr. Opin. Struct. Biol.* **1997**, *7*, 566–573.

(10) Aroian, R.; van der Goot, F. G. Pore-forming toxins and cellular non-immune defenses (CNIDs). *Curr. Opin. Microbiol.* **2007**, *10*, 57–61.

(11) Anderluh, G.; Krizaj, I.; Strukelj, B.; Gubensek, F.; Macek, P.; Pungercar, J. Equinatoxins, pore-forming proteins from the sea anemone *Actinia equina*, belong to a multigene family. *Toxicon* **1999**, *37*, 1391–1401.

(12) Athanasiadis, A.; Anderluh, G.; Macek, P.; Turk, D. Crystal structure of the soluble form of equinatoxin II, a pore-forming toxin from the sea anemone *Actinia equina*. *Structure* **2001**, *9*, 341–346.

(13) Lanio, M. E.; Morera, V.; Álvarez, C.; Tejuca, M.; Gómez, T.; Pazos, F.; Besada, V.; Martínez, D.; Huerta, V.; Padrón, G.; Chávez, M. A. Purification and characterization of two hemolysins from *Stichodactyla helianthus*. *Toxicon* **2001**, *39*, 187–194.

(14) Bellomio, A.; Morante, K.; Barlic, A.; Gutiérrez-Aguirre, I.; Viguera, A. R.; González-Mañas, J. M. Purification, cloning and characterization of fragaceatoxin C, a novel actinoporin from the sea anemone *Actinia fragacea*. *Toxicon* **2009**, *54*, 869–880.

(15) Hong, Q.; Gutiérrez-Aguirre, I.; Barlic, A.; Malovrh, P.; Kristan, K.; Podlesek, Z.; Macek, P.; Turk, D.; González-Mañas, J. M.; Lakey, J. H.; Anderluh, G. Two-step membrane binding by equinatoxin II, a pore forming toxin from the sea anemone, involves an exposed aromatic cluster and a flexible helix. *J. Biol. Chem.* **2002**, *277*, 41916–41924.

(16) Alegre-Cebollada, J.; Oñaderra, M.; Gavilanes, J. G.; Martínez del Pozo, A. Sea Anemone Actinoporins: The transition from a folded soluble state to a functionally active membrane-bound oligomeric pore. *Curr. Protein Pept. Sci.* **2007**, *8*, 558–572.

(17) Tanaka, R.; Caaveiro, J. M. M.; Morante, K.; González-Mañas, J. M.; Tsumoto, K. Structural basis for self-assembly of a cytolytic pore lined by protein and lipid. *Nat. Commun.* **2015**, *6*, 6337.

(18) Barlic, A.; Gutiérrez-Aguirre, I.; Caaveiro, J. M. M.; Cruz, A.; Ruiz-Argüello, M. B.; Pérez-Gil, J.; González-Mañas, J. M. Lipid phase coexistence favors membrane insertion of equinatoxin-II, a pore-forming toxin from *Actinia equina*. *J. Biol. Chem.* **2004**, *279*, 34209–34216.

(19) Martínez, D.; Otero, A.; Álvarez, C.; Pazos, F.; Tejuca, M.; Lanio, M. E.; Gutiérrez-Aguirre, I.; Barlic, A.; Iloro, I.; Arrondo, J. L.; González-Mañas, J. M.; Lissi, E. Effect of sphingomyelin and cholesterol on the interaction of St II with lipidic interfaces. *Toxicon* **2007**, *49*, 68–81.

(20) Schön, P.; García-Sáez, A. J.; Malovrh, P.; Bacia, K.; Anderluh, G.; Schwill, P. Equinatoxin II Permeabilizing Activity Depends on the presence of Sphingomyelin and Lipid Phase Coexistence. *Biophys. J.* **2008**, *95*, 691–698.

(21) García-Sáez, A. J.; Buschhorn, S. B.; Keller, H.; Anderluh, G.; Simons, K.; Schwill, P. Oligomerization and Pore Formation by



Equinatoxin II Inhibit Endocytosis and Lead to Plasma Membrane Reorganization. *J. Biol. Chem.* **2011**, *286*, 37768–37777.

(22) Rojko, N.; Cronin, B.; Danial, J. S. H.; Baker, M. A. B.; Anderluh, G.; Wallace, M. I. Imaging the Lipid-Phase-Dependent Pore Formation of Equinatoxin II in Droplet Interface Bilayers. *Biophys. J.* **2014**, *106*, 1630–1637.

(23) García-Linares, S.; Alm, I.; Maula, T.; Gavilanes, J. G.; Slotte, J. P.; Martínez-del-Pozo, A. The Effect of Cholesterol on the Long-Range Network of Interactions Established among Sea Anemone Sticholysin II Residues at the Water-Membrane Interface. *Mar. Drugs* **2015**, *13*, 1647–1665.

(24) de Almeida, R. F.; Fedorov, A.; Prieto, M. Sphingomyelin/phosphatidylcholine/cholesterol phase diagram: boundaries and composition of lipid rafts. *Biophys. J.* **2003**, *85*, 2406–2416.

(25) Pedrera, L.; Fanani, M. L.; Ros, U.; Lanio, M. E.; Maggio, B.; Álvarez, C. Sticholysin I–membrane interaction: An interplay between the presence of sphingomyelin and membrane fluidity. *Biochim. Biophys. Acta, Biomembr.* **2014**, *1838*, 1752–1759.

(26) Beattie, M. E.; Veatch, S. L.; Stottrup, B. L.; Keller, S. L. Sterol Structure Determines Miscibility versus Melting Transitions in Lipid Vesicles. *Biophys. J.* **2005**, *89*, 1760–1768.

(27) Ahn, K. W.; Sampson, N. S. Cholesterol oxidase senses subtle changes in lipid bilayer structure. *Biochemistry* **2004**, *43*, 827–836.

(28) Xu, X.; Bittman, R.; Duportail, G.; Heissler, D.; Vilcheze, C.; London, E. Effect of the Structure of Natural Sterols and Sphingolipids on the Formation of Ordered Sphingolipid/Sterol Domains (Rafts). *J. Biol. Chem.* **2001**, *276*, 33540–33546.

(29) Bianco, I. D.; Maggio, B. Interactions of neutral and anionic glycosphingolipids with dilauroylphosphatidylcholine and dilauroylphosphatidic acid in mixed monolayers. *Colloids Surf.* **1989**, *40*, 249–260.

(30) Brockman, H. L.; Jones, C. M.; Schwebke, C. J.; Smaby, J. M.; Jarvis, D. E. Application of microcomputer-controlled film balance system to collection and analysis of data from mixed monolayers. *J. Colloid Interface Sci.* **1980**, *78*, 502–512.

(31) Wilke, N.; Maggio, B. The influence of domain crowding on the lateral diffusion of Ceramide-enriched domains in a Sphingomyelin monolayer. *J. Phys. Chem. B* **2009**, *113*, 12844–12851.

(32) Wilke, N.; Vega Mercado, F.; Maggio, B. Rheological Properties of a Two Phase Lipid Monolayer at the Air/Water Interface: Effect of the Composition of the Mixture. *Langmuir* **2010**, *26* (13), 11050–11059.

(33) Hughes, D.; Pailthorpe, B.; White, L. The translational and rotational drag on a cylinder moving in a membrane. *J. Fluid Mech.* **1981**, *110*, 349–372.

(34) Martínez, D.; Campos, A. M.; Pazos, F.; Álvarez, C.; Lanio, M. E.; Casallanovo, F.; Schreier, S.; Salinas, R. K.; Vergara, C.; Lissi, E. Properties of St I and St II, two isotoxins isolated from *Stichodactyla helianthus*: a comparison. *Toxicon* **2001**, *39*, 1547–1560.

(35) Ale, E. C.; Maggio, B.; Fanani, M. L. Ordered-disordered domain coexistence in ternary lipid monolayers activates sphingomyelinase by clearing ceramide from the active phase. *Biochim. Biophys. Acta, Biomembr.* **2012**, *1818*, 2767–2776.

(36) De Tullio, L.; Maggio, B.; Fanani, M. L. Sphingomyelinase acts by an area-activated mechanism on the liquid-expanded phase of sphingomyelin monolayers. *J. Lipid Res.* **2008**, *49*, 2347–2355.

(37) Angelova, M. I.; Dimitrov, D. S. Liposomes electroformation. *Faraday Discuss. Chem. Soc.* **1986**, *81*, 303–311.

(38) Goñi, F. M.; Alonso, A.; Bagatolli, L. A.; Brown, R. E.; Marsh, D.; Prieto, M.; Thewalt, J. L. Phase diagrams of lipid mixtures relevant to the study of membrane raft. *Biochim. Biophys. Acta, Mol. Cell Biol. Lipids* **2008**, *1781*, 665–684.

(39) Stottrup, B. L.; Stevens, D. S.; Keller, S. L. Miscibility of Ternary Mixtures of Phospholipids and Cholesterol in Monolayers, and Application to Bilayer Systems. *Biophys. J.* **2005**, *88*, 269–276.

(40) Fanani, M. L.; Maggio, B. Liquid-liquid domain miscibility driven by composition and domain thickness mismatch in ternary lipid monolayers. *J. Phys. Chem. B* **2011**, *115*, 41–49.

(41) Maget-Dana, R. The monolayer technique: a potent tool for studying the interfacial properties of antimicrobial and membrane-lytic peptides and their interactions with lipid membranes. *Biochim. Biophys. Acta, Biomembr.* **1999**, *1462*, 109–140.

(42) Brockman, H. Lipid monolayers: why use half a membrane to characterize protein-membrane interactions? *Curr. Opin. Struct. Biol.* **1999**, *9*, 438–443.

(43) Phillips, M. C.; Graham, D. E.; Hauser, H. Lateral compressibility and penetration into phospholipid monolayers and bilayer membranes. *Nature (London, U. K.)* **1975**, *254*, 154–156.

(44) Smaby, J. M.; Momsen, M. M.; Brockman, H. L.; Brown, R. E. Phosphatidylcholine acyl unsaturation modulates the decrease in interfacial elasticity induced by cholesterol. *Biophys. J.* **1997**, *73*, 1492–1505.

(45) Smaby, J. M.; Kulkarni, V. S.; Momsen, M.; Brown, R. E. The interfacial elastic packing interactions of galactosylceramides, sphingomyelins, and phosphatidylcholines. *Biophys. J.* **1996**, *70*, 868–877.

(46) Li, X. M.; Smaby, J. M.; Momsen, M. M.; Brockman, H. L.; Brown, R. E. Sphingomyelin interfacial behavior: the impact of changing acyl chain composition. *Biophys. J.* **2000**, *78*, 1921–1931.

(47) Stottrup, B. L.; Keller, S. L. Phase behavior of lipid monolayers containing DPPC and cholesterol analogs. *Biophys. J.* **2006**, *90*, 3176–3183.

(48) Caruso, B.; Mangiarotti, A.; Wilke, N. Stiffness of Lipid Monolayers with Phase Coexistence. *Langmuir* **2013**, *29*, 10807–10816.

(49) Tejuca, M.; Dalla Serra, M.; Potrich, C.; Álvarez, C.; Menestrina, G. Sizing the radius of the pore formed in erythrocytes and lipid vesicles by the toxin sticholysin I from the sea anemone *Stichodactyla helianthus*. *J. Membr. Biol.* **2001**, *183*, 125–135.

(50) Kuga, S. Pore size distribution analysis of gel substances by size exclusion chromatography. *J. Chromatogr.* **1981**, *206*, 449–461.

(51) Schultz, S. G.; Solomon, A. K. Determination of the effective hydrodynamic radii of small molecules by viscometry. *J. Gen. Physiol.* **1961**, *44*, 1189–1199.

(52) Ferdani, R.; Li, R.; Pajewski, R.; Pajewska, J.; Winter, R. K.; Gokel, G. W. Transport of chloride and carboxyfluorescein through phospholipid vesicle membranes by heptapeptide amphiphiles. *Org. Biomol. Chem.* **2007**, *5* (15), 2423–2432.

(53) Alm, I.; García-Linares, S.; Gavilanes, J. G.; Martínez-del-Pozo, A.; Slotte, J. P. Cholesterol stimulates and ceramide inhibits Sticholysin II-induced pore formation in complex bilayer membranes. *Biochim. Biophys. Acta, Biomembr.* **2015**, *1848*, 925–931.

(54) Cournia, Z.; Ullmann, G. M.; Smith, J. C. Differential Effects of Cholesterol, Ergosterol and Lanosterol on a Dipalmitoyl Phosphatidylcholine Membrane: A Molecular Dynamics Simulation Study. *J. Phys. Chem. B* **2007**, *111*, 1786–1801.

(55) Yasuda, T.; Tsuchikawa, H.; Murata, M.; Matsumori, N. Deuterium NMR of Raft Model Membranes Reveals Domain-Specific Order Profiles and Compositional Distribution. *Biophys. J.* **2015**, *108*, 2502–2506.

(56) Alvarez-Valcárcel, C.; Dalla Serra, M.; Potrich, C.; Bernhart, I.; Tejuca, M.; Martínez, D.; Pazos, F.; Lanio, M. E.; Menestrina, G. Effects of Lipid Composition on Membrane Permeabilization by Sticholysin I and II, Two Cytolysins of the Sea Anemone *Stichodactyla helianthus*. *Biophys. J.* **2001**, *80*, 2761–2774.

(57) Anderluh, G.; Dalla-Serra, M.; Viero, V.; Guella, G.; Macek, P.; Menestrina, G. Pore formation by Equinatoxin II, a eukaryotic protein toxin, occurs by induction of nonlamellar lipid structures. *J. Biol. Chem.* **2003**, *278*, 45216–45223.

(58) Seddon, J. M. Structure of the inverted hexagonal ( $H_{II}$ ) phase, and non-lamellar phase transitions of lipids. *Biochim. Biophys. Acta, Rev. Biomembr.* **1990**, *1031*, 1–69.

(59) Israelachvili, J.; Marcelja, S.; Horn, R. Physical principles of membrane organization. *Q. Rev. Biophys.* **1980**, *13*, 121–200.

(60) Carnie, S.; Israelachvili, J. N.; Pailthorpe, B. A. Lipid packing and transbilayer asymmetries of mixed lipid vesicles. *Biochim. Biophys. Acta, Biomembr.* **1979**, *554*, 340–357.

(61) Kumar, V. V. Complementary molecular shapes and additivity of the packing parameter of lipids. *Proc. Natl. Acad. Sci. U. S. A.* **1991**, 88, 444–448.

(62) Gallay, J.; De Kruijff, B. Correlation between molecular shape and hexagonal H<sub>II</sub> phase promoting ability of sterols. *FEBS Lett.* **1982**, 143, 133–136.